RSC Advances

PAPER

View Article Online
View Journal | View Issue

Cite this: *RSC Adv.*, 2026, **16**, 23922

Waste water remediation through ultrafast reduction of organic dyes, nitroaromatics, and nitrofuran antibiotics employing efficient multifunctional rGO/Ni-MOF composites

Richa Tiwari,[a] Akhilesh Kumar,[a] Sneha Naik,[b] Archi Jain,[a] Asmita Singh,[a] Narendra Pal Lamba,[a] Sonia Chahar Srivastava*[c] and Manmohan Singh Chauhan *[d]

Received 3rd January 2026
Accepted 4th February 2026

DOI: 10.1039/d6ra00044d

rsc.li/rsc-advances

Herein, we report a synthesis of a highly efficient and effective Ni-MOF/GO composite catalyst and its application in the reduction of nitroaromatic compounds, dyes, and nitrofuran antibiotics (nitrofurantoin). The composite was prepared *via* a sonication-assisted method, effectively integrating a nickel metal–organic framework (Ni-MOF) onto graphene oxide (GO) sheets. The catalytic performance of the Ni-MOF/GO composite was well evaluated in the reduction of nitroaromatics such as *p*-nitrophenol, picric acid, and *p*-nitroaniline and dyes using sodium borohydride ($NaBH_4$) as a reducing agent, under milder conditions, thus highlighting its structural properties and potential as a highly effective catalyst for remediation of waste water from industrial processes. Furthermore, the Ni-MOF/GO composite is used for the degradation of nitro-containing antibiotics, such as nitrofurans, in medical effluents. Degraded nitrofurantoin was investigated for its antibacterial activity to assess the drug-resistant capacity of bacteria. The catalyst was characterized using XRD, FTIR, SEM, and TEM.

1. Introduction

Recent years have seen a significant increase in attention given to the problem of ecological contamination brought on by the industry's rapid technological advancements.[1–5] For instance, nitrophenols are essential industrial chemicals, but when they end up in water, they can poison aquatic life and humans severely. By chemical reduction, these molecules can be converted into aminophenols, thus offering a variety of alternate uses.[6–8] In general, aromatic amines are comparatively safer chemicals with a wide range of biological and synthetic applications, such as improving photography, producing dye intermediates, optical brighteners, inhibiting corrosion, lubricating against corrosion, and using pharmaceuticals to make drugs.[9–11] In industries such as textiles, paper, food, and pharmaceuticals, the reduction of nitroarenes and dyes has become a crucial and transformative process.[12–14] Various approaches, including oxidation and degradation, have been employed to eliminate 4-nitrophenol (4-NP) and other organic molecules from the environment.[15–18] But these methods have proven to be costly and only partially effective.

However, because of their great visibility, resistance to deterioration, and unsightliness, as well as the pollution of wastewater, their excessive use has led to environmental damage. Thus, maintaining a clean and safe environment requires strict management over industrial effluents. Known by several names, including 5,5′-indigodisulfonic acid di sodium salt, and categorized as a vat dye. Indigo carmine dye is a basic organic blue dye that has been used for thousands of years as a pigmenting agent with high absorptivity.[19] On the other hand, one- or two-electron oxidants can oxidize it.[20,21] These dyes are easily obtained from the market, reasonably priced, stable, and very soluble in aqueous solutions and mildly soluble in organic solvents. Its durability as a colorant is also explained by the fact that indigo dye is among the most stable organic dyes.[22,23] The blue-colored substance gradually deteriorates into a colorless product as a result of exposure to light, humidity, and oxidizing chemicals over time. Alizarin red S (ARS), also known as 1,2-dihydroxy-9,10-anthraquinonesulfonic acid sodium salt, is a water-soluble anthraquinone dye that was first made from the madder plant's root.[24] It has been widely used to color textiles from prehistoric times.[25] Since it is a potent oxidizer, heat and moisture should be kept away from it when storing.[26] For coloring and disinfection purposes, methylene blue (MB) and malachite green (MG) are frequently employed in industries such as fish farming, paper, leather, pulp, and textiles.[27] However, according to Ngamsurach *et al.*, the release of wastewater with high dye concentrations into water bodies results in serious environmental harm.[28]

[a]*Amity University Rajasthan, Jaipur 303002, India*
[b]*Department of Chemistry, Carmel College for Women, Goa 403601, India*
[c]*S.S. Jain Subodh P.G. (Autonomous) College, Jaipur 302005, India. E-mail: soniachahar@gmail.com*
[d]*Department of Chemistry, Central University of Rajasthan, Kishangarh 305817, India. E-mail: manmohan.chauhan@curaj.ac.in*

Heterogeneous catalysis may provide a better solution for such environmental issues including many benefits, such as great stability and reusability, high catalytic activity, and high selectivity due to a broad surface area.[29] The surface area characteristics and shape-adjusted catalytic activity of nanoparticle-based heterogeneous catalysts make them very interesting. Recently, silver nanoparticle based composite reported for reduction of nitro aromatics, nitrofurantoin and their biological activity.[30–35] Noble metals have excellent catalytic activity, but their application is limited due to their high economic cost.[36]

To get over these restrictions, transition metal catalysts have been used extensively in its stead. These catalysts were used in several transformations, including oxidations;[37–41] breakdown of dyes like eosin Y and methylene blue;[42] 2,4-dimethyl phenol;[43] orange (II);[44] and crystal violet dye.[45] Because of its superior surface characteristics, graphene oxide (GO) is a viable option for supporting transition-metal catalysts to enhance their catalytic activity.[46] Positive operation of GO as a support for both stabilizing and dispersing metal nanoparticles has been demonstrated.[47] GO is used as a substrate for the synthesis of water-soluble nanocarbon because of its favorable dispersion in aqueous solution. Nevertheless, the porous metal–organic framework (MOF) is another fascinating nanomaterial with built-in qualities including great stability, strength under challenging conditions, and easy accessibility. MOFs have a variety of tunable features, including structure, density, and surface area.[48,49] They are made up of inorganic metal ions and organic linkers, or ligands. These MOFs are used for catalytic activity, medication administration, and gas storage.[50–55] Building upon prior research, our work reports a simple, efficient, cost-effective and environmentally benign catalyst Ni-MOF/GO composite for reduction of nitroaromatic compounds, dye, and antibiotic drug (nitrofurantoin). The catalyst was synthesized by dispersing graphene oxide (GO) in a nickel nitrate solution with trimesic acid *via* a sonication process. Our findings demonstrate the application of synthesized Ni-MOF/GO composite for the reduction of differently substituted nitroaromatic compounds dyes, and antibiotic drugs (nitrofurantoin). Our prepared catalyst offers significant improvements in the reduction of nitroaromatic pollutants, presenting a more efficient alternative compared to the conventional Ni-based catalyst.

2. Experimental

2.1 Chemicals and reagents

The following were purchased from CDH Chemicals (company) graphite powder, HCl, H_2SO_4 (98%), NaOH, NH_4Cl, and $Ni(NO_3)_2\cdot 6H_2O$. CDH Chemicals provided anhydrous ethanol, acetic acid (HAc), and *N*,*N*-dimethylformamide (DMF). CDH chemicals (Company) supplied trimesic acid (H_3BTC). Analytical grade reagents and chemicals were all used without further purification.

2.2 Apparatus

Using a powder X-ray diffractometer (XRD, Dmax1400, Rigaku Company, Japan) with a Cu Kα radiation source of $\lambda = 0.154060$ Å and a 2θ angle range of 0° to 100°, the crystal structure and phase purity information of the materials were determined. KBr pellets were used to capture infrared spectra of materials in the wavenumber range of 4000–400 cm^{-1} using a Fourier transform infrared spectrometer (FT-IR, Spectrum Two N, PerkinElmer Company, America). Materials' Raman spectra were captured using a Raman spectrometer (inVia, Renishaw Instrument Co., Britain) that was exposed to laser light between 650 and 2000 cm^{-1}. Scanning electron microscopy (SEM, Sigma 500, Carl Zeiss AG, Germany) was used to examine the microstructure and morphology of the materials.

2.3 Synthesis of catalyst

2.3.1 Preparation of graphene oxide (GO).[56] Graphene oxide (GO) was prepared using a modified Hummer's Method (Scheme 1), where 200 mg of graphite powder, 100 mg of sodium nitrate $NaNO_3$, and 5 ml of concentrated sulfuric acid (H_2SO_4) were mixed and cooled to 0 °C. The mixture was stirred, and 600 mg of potassium permanganate ($KMnO_4$) was added while maintaining the temperature below 20 °C. After 30 minutes, the temperature gradually increased to 35 °C, and the solution turned brown upon adding 10 mL of distilled water.

Subsequent addition of water raised the temperature to 98 °C and was maintained for 15 minutes. Then, 500 mL of 3% hydrogen peroxide (H_2O_2) and 28 mL of warm distilled water were mixed into the solution. The resulting light-yellow suspension was thoroughly washed 7–8 times with distilled water and air-dried. 20 ml of distilled water was added to the precipitate obtained and sonicated for 15 minutes. The solution was then centrifuged for 30 minutes at 3000 rpm, and the graphene oxide (GO) solution was collected from the supernatant. The solution was vacuum-dried to obtain GO in powder form.

2.3.2 Catalyst preparation – synthesis of Ni-MOF/GO composite.[57] GO and $Ni(NO_3)_2\cdot 6H_2O$ (10 mmol) was added in 80 ml of mixture of anhydrous ethanol and distilled water (1 : 1 v/v ratio). The reaction mixture allowed to ultrasonication for 50 minutes to dissolve the $Ni(NO_3)_2\cdot 6H_2O$. H_3BTC was added to this mixture and was stirred for 60 minutes at room temperature. NaOH (15 mmol) was added in this mixture to develop the Ni-MOF/GO composite and further stirred for 60 minutes (Scheme 2). The precipitate was collected and washed with distilled water and anhydrous ethanol, and the final black powder obtained was kept for drying at 60 °C for 12 hours.

2.4 Catalytic performance

2.4.1 Reduction of nitro-aromatic compounds and dyes. Ni-MOF/GO composite used as a catalyst for reduction of nitroaromatic compounds like *p*-nitrophenol (PNP), *p*-nitroaniline (PNA), and picric acid in presence of $NaBH_4$ as the reducing agent and monitored using UV-vis spectroscopic technique. First, the reduction of PNP to *p*-aminophenol at room temperature was selected as a model reaction to evaluate the catalytic activity of Ni-MOF/GO composite. Initially, catalyst is added into aqueous solution of PNP (14 mg in 10 ml) followed by the addition of an aqueous solution of 1 ml of $NaBH_4$ (38 mg in 1 ml) (Scheme 3). After complete reduction, the yellow colour of the reaction mixture turned colourless, thus indicating

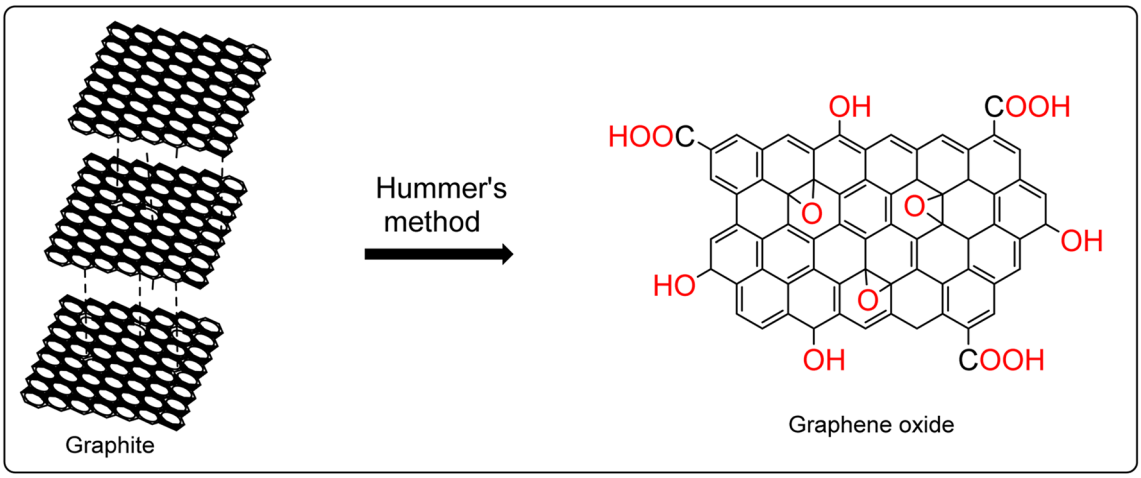

Scheme 1 Preparation of graphene oxide.

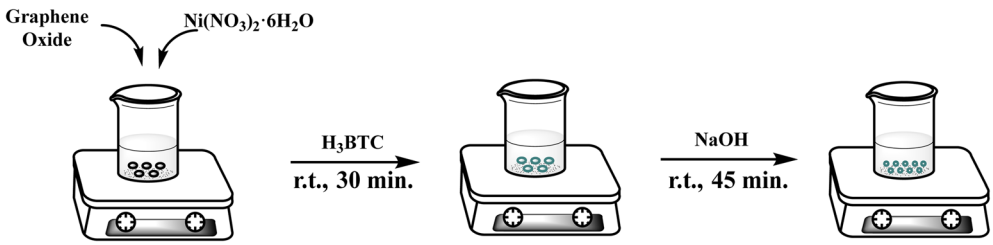

Scheme 2 Schematic representation for the synthesis of Ni-MOF/GO composite.

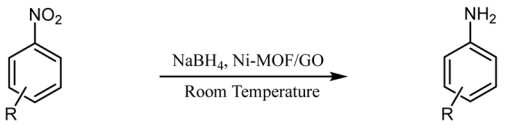

Scheme 3 Catalytical reduction reaction of nitroaromatic compound.

a successful conversion of PNP to *p*-aminophenol. Similar procedure was used for the reduction of PNA, and picric acid. In general, 30 mg of catalyst is added into aqueous solution (10 mL) of nitro compounds-PNA (0.1 mmol, 14 mg), and picric acid (0.1 mmol, 23 mg) separately along with an aqueous solution of sodium borohydride (0.1 mmol, 38 mg), allow to stirring it at room temperature. The reduction of these nitro aromatic compounds was monitored using UV spectroscopy.

The percentage reduction of nitro aromatic compounds was calculated by eqn (1) given below:

$$\%\ \text{Reduction or}\ \%\ \text{degradation} = \frac{C_i - C_f}{C_i} \times 100 \quad (1)$$

where C_i and C_f are the initial and final concentrations of nitro aromatic compounds.

The same procedure is used for the reduction of dyes like methylene and malachite green.

2.4.2 Analysis of antibiotic activity of nitrofurantoin. Analysis of antibiotic activity before and after reduction of nitrofurantoin by the Ni-MOF/GO was performed using the disk diffusion method. *E. coli* bacteria growing in their log phase were evenly spread over a Luria–Bertani (LB) agar plate. Autoclaved disks made of Whatman paper (diameter 6 mm) were placed on the LB plate, and 10 μl of solution containing either 10 or 20 ppm of nitrofurantoin was incubated for 5 minutes with either $NaBH_4$, Ni-MOF alone, or $NaBH_4$ and Ni-MOF both. The plate was incubated overnight at 37 °C. The zone of inhibition around the paper disk was visualized the next day, and the radius of the zone of inhibition was measured as a function of antibiotic activity.

3. Results and discussion

3.1 XRD analysis

XRD tests were performed to analysis the information of crystal structure and phase purity of as-prepared Ni-MOF/GO composite. As showing in Fig. 1, a broad peak around $2\theta = 10°$–$12°$ attributed to graphene oxide sheet while peak around $2\theta = 20°$ attributed for BTC linker indicating its incorporation within the MOF matrix. Peak around 38.0°, 43.3°, 62.0°, 73.9°, and 79.5° corresponding to the reflection planes of (111), (200), (220), (311), (222) of cubic NiO (JCPDS no.47-1049) respectively[58] confirming the presence of well defined nickel within the composite. The combined presence of diffraction peaks in the 2θ range of 1–30° [59] confirming the successful incorporation of MOF-derived nickel species onto the GO framework.

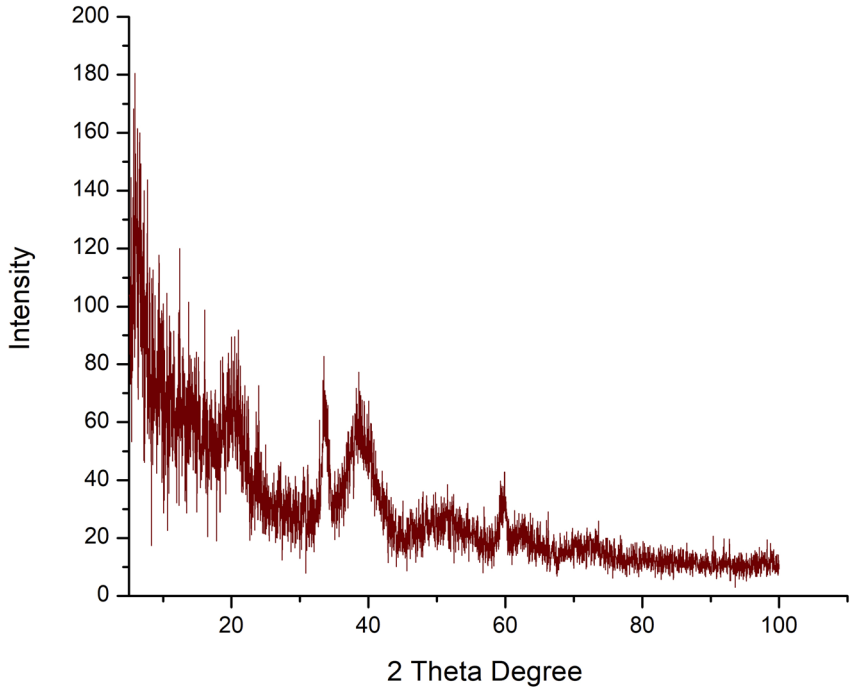

Fig. 1 XRD pattern of Ni-MOF/GO composite.

3.2 FT-IR analysis

The FTIR spectrum of the Ni-MOF/GO composite and its precursor Ni-MOF (Fig. 2 and 3) revealed characteristic vibrational modes. The Ni-MOF (Fig. 2) displays characteristic peaks associated with the coordination between H_3BTC and Ni ions.[52,53] The peaks around 1610 cm^{-1} and 1368 cm^{-1} correspond to the asymmetric and symmetric stretching vibrations of the carboxylate groups, confirming the interaction between the metal ions and the carboxylate ligands of H_3BTC. Additional peaks in the range of 3400 cm^{-1} represent hydroxyl (O–H) vibrations and may be attributed to moisture or remaining carboxylate ligands.[54–56]

The FTIR spectrum of the Ni-MOF/GO composite (Fig. 3) shows similar bands to the Ni-MOF spectrum, indicating that the incorporation of graphene oxide (GO)[58,59] does not significantly affect the coordination between H_3BTC and nickel ions. However, the broad band between 3225 cm^{-1} can be attributed to the hydroxyl groups (O–H) present in GO.[56,59] This indicates the presence of oxygen-containing functional groups from GO, which may slightly modify the overall structure. Band related to –C–O group occur at 1431 cm^{-1} and 1360 cm^{-1}, indicating that the BTC coordinated with Ni. Peaks related to C=O stretching vibrations from carboxyl groups in GO are also observed around 1610 cm^{-1}.[60]

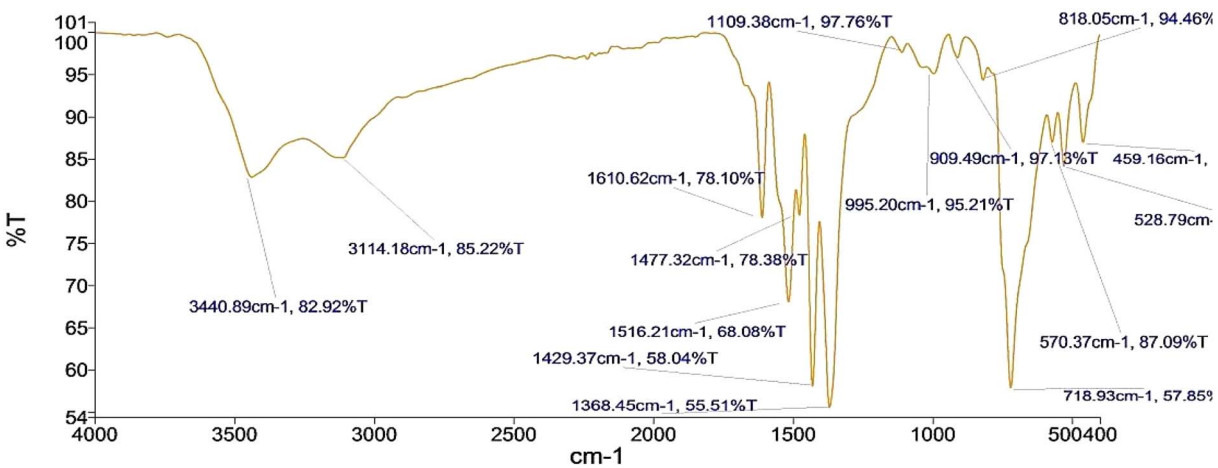

Fig. 2 FTIR graph of Ni-MOF composite.

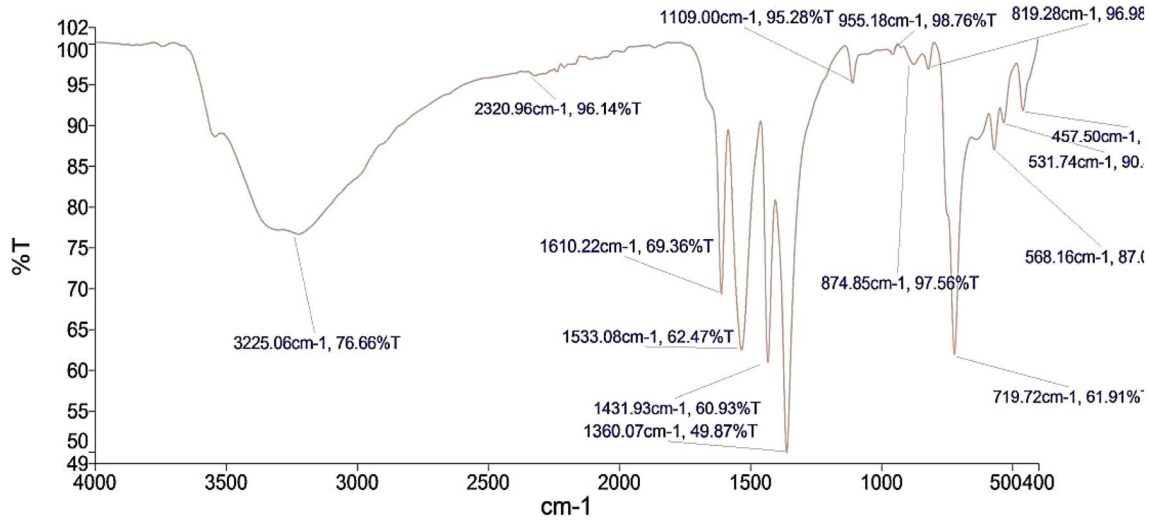

Fig. 3 FTIR graph of Ni-MOF/GO composite.

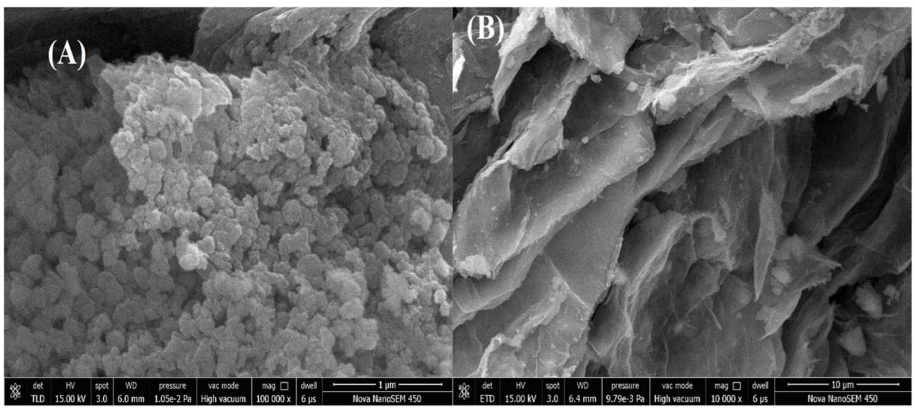

Fig. 4 (A) SEM images of Ni-MOF, (B) SEM images of Ni-MOF/GO composite.

3.3 SEM analysis

Fig. 4(A and B)are SEM images of Ni-MOF and Ni-MOF/GO composite respectively. Ni-MOF (Fig. 4(A)) exhibited a morphology of aggregated spherical particles forming a relatively structure. The particle show a rough and porous structure which is beneficial for enhance the surface area and it also

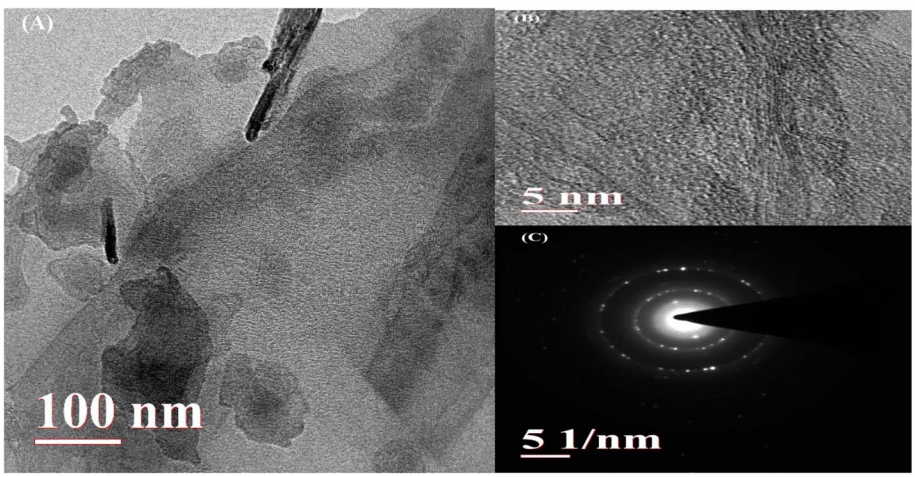

Fig. 5 (A and B) TEM images of Ni-MOF/GO composite, (C) SAED.

Table 1 Optimisations for reduction of pollutants

Pollutants	Concentration of the pollutants	Composition of the composites or nanoparticles	Concentration of $NaBH_4$	Time (minutes)
4-Nitroaniline	14 mg (0.1 mmol)	10 mg	19 mg	03:25
4-Nitroaniline	14 mg (0.1 mmol)	20 mg	19 mg	01:54
4-Nitroaniline	14 mg (0.1 mmol)	30 mg	19 mg	01:05
4-Nitroaniline	14 mg (0.1 mmol)	30 mg	28 mg	00:35
4-Nitroaniline	14 mg (0.1 mmol)	30 mg	38 mg	00:25
Picric acid	23 mg (0.1 mmol)	30 mg	38 mg	00:45
4-Nitrophenol	14 mg (0.1 mmol)	30 mg	38 mg	01:10
Methylene blue	100 ppm	30 mg	38 mg	Instantaneous
Malachite green	100 ppm	30 mg	38 mg	Instantaneous

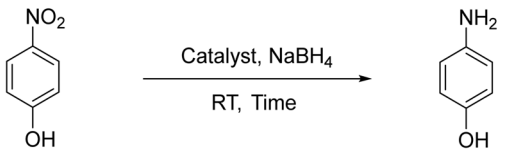

Scheme 4 Catalytic reduction of 4-nitrophenol.

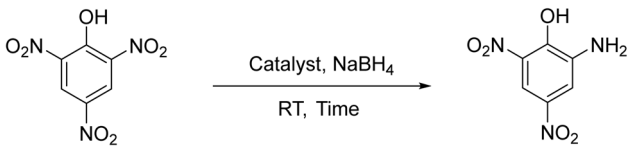

Scheme 5 Catalytic reduction of picric acid.

promotes the catalytic sites. Such type of morphology further indicates the formation of nickel based nano-domains during the synthesis and growth on the support. As shown in Fig. 4(B), the layered structure of graphene oxide (GO) depicted. The sheet like morphology confirm the 2D structure of GO which providing the high surface area for anchoring of Ni-MOF. The spherical particles of Ni-MOF are scattered on the surface of these wrinkle-like and flakes of GO sheets thus enhancing the catalytic properties of composite.

3.4 TEM analysis

The TEM analysis of the Ni-MOF/GO composite (Fig. 5 A–C) confirms the successful integration of Ni-MOF nanoparticles onto the GO sheets. Fig. 5(A) shows the presence of dispersed Ni-MOF anchored onto the GO sheet. It also confirms the interaction in between metallic species and GO matrix. Fig. 5(B) reveals the crystalline nature of Ni-MOF and shows the clear lattice fringes with interplanar spacing corresponding to characteristic plane of nickel supported on GO framework. Such structural order supports the active catalytic sites with high stability. SAED pattern (5C), suggests the polycrystalline nature of Ni-MOF. The sheet-like structure of GO provides support for the Ni-MOF particles while maintaining structural integrity, and

Table 2 Optimization table for reduction of 4-nitrophenol

Sr. no.	Substrate (mg)	Catalyst loading	$NaBH_4$ (mg)	Time (min)
1	14 mg	30 mg	19	01:40
2	14 mg	30 mg	28	01:22
3	14 mg	30 mg	38	01:10
4	14 mg	20 mg	19	23:00
5	14 mg	20 mg	28	20:00
6	14 mg	20 mg	38	15:00
7	14 mg	10 mg	19	65:00
8	14 mg	10 mg	28	50:00
9	14 mg	10 mg	38	30.00
10	14 mg	No catalyst	19	No reaction

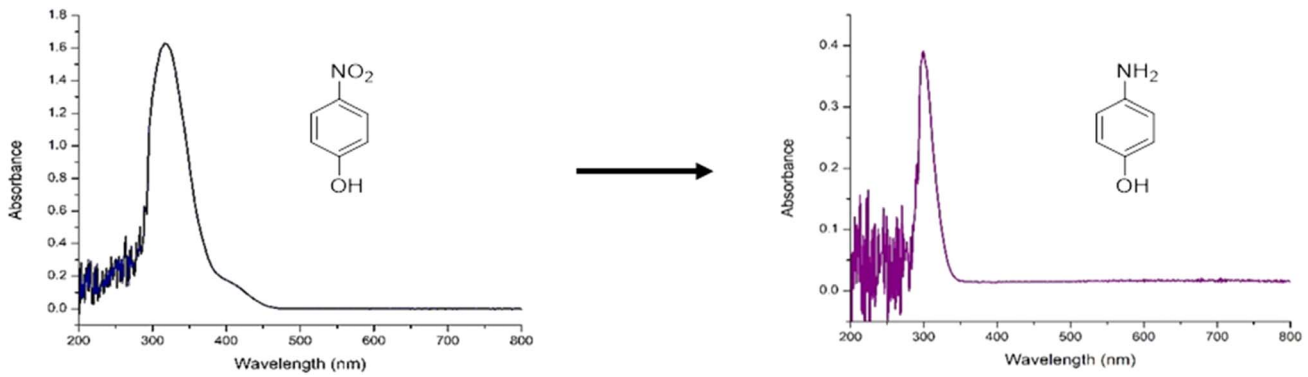

Fig. 6 Reduction of PNP to *p*-aminophenol.

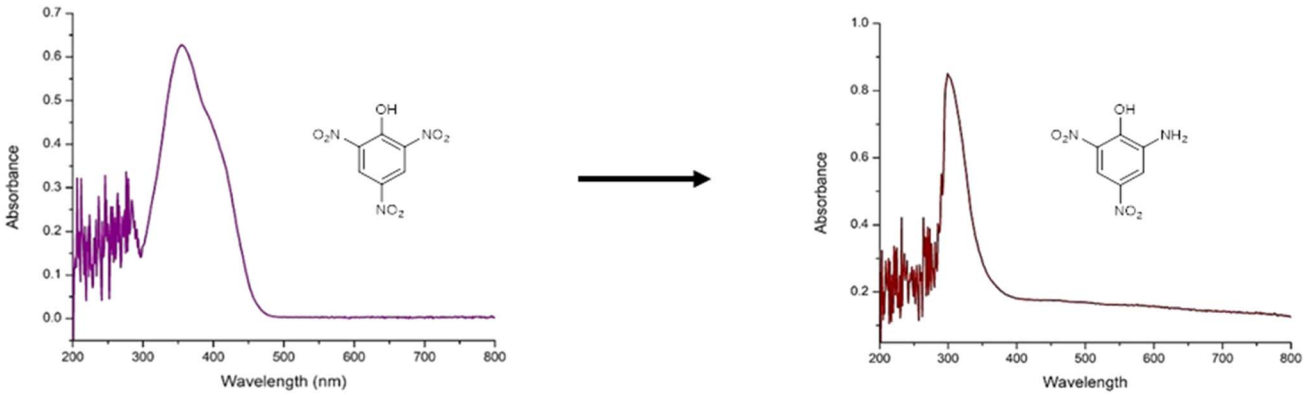

Fig. 7 Reduction of picric acid to picramic acid.

the small particle size of the Ni-MOF enhances the potential for catalytic applications.

4. Catalytic reduction of nitro compounds

The reduction of nitro group is a significant and difficult chemical process. Nitro substrates are used in a wide range of applications, such as dyes, insecticides, and herbicides. As a result of their essential function in the textile, dye, and agricultural industries, these substrates eventually harm or poison the environment. Nitroaromatics may have an impact due to their enduring presence in the environment. The creation of safer products through the breakdown or reduction of these nitro compounds is therefore crucial. We have screened different types of nitro aromatic compounds for the reduction reaction in the presence of Ni-MOF/GO composite.

Ni-MOF/GO composite catalyst was used for reduction of 4-nitrophenol (PNP), picric acid, 4-nitroaniline (PNA) dyes like malachite green, methylene blue. Reduction of all these compounds were analysed by using UV-visible spectroscopy. The Ni-MOF/GO composite demonstrated excellent catalytic performance across all the nitroaromatic compounds tested as shown in Table 1. Firstly, pH of aqueous solution become basic due to interaction of nitroaromatics with freshly prepared $NaBH_4$ and colour changed from bright yellow to dazzling yellow.[61] Additionally, aqueous solution of nitroaromatics produced large number of gas bubbles which released during reaction.[62] In the absence of catalyst, absorption peak of nitroaromatics remains constant after 30 minutes, which indicating that $NaBH_4$ not able to efficiently reduce nitroaromatics in the absence of an active catalyst.[63] As well as catalyst quantity increases, the required time for reduction of nitroaromatics decreases. Dyes like methylene blue and malachite green reduced instantaneous with 30 mg of catalyst and 38 mg of $NaBH_4$. The catalytic efficiency can be attributed to the large surface area provided by the GO sheets, which facilitates the uniform distribution of Ni-MOF nanoparticles and enhances the interaction between the reactants and catalyst. The small particle size of Ni-MOF further contributed to the increased surface area and active sites available for the reduction reactions. The optimized reaction conditions for the reduction of nitroaromatics involved using 30 mg of Ni-MOF/GO catalyst and 38 mg of $NaBH_4$, providing the best balance between catalyst loading, $NaBH_4$ amount, and reaction time (Schemes 4 and 5).

4.1 *p*-Nitrophenol

The reduction of nitrophenol is monitored by UV-vis spectroscopy. Nitro compound does not reduce in the absence of metal catalyst. In the presence of metal catalyst, nitro compound getting reduced and show absorption at 400 nm, which is due to the formation of the *p*-nitrophenolate ion.[64] As shown in Fig. 6,

Table 3 Optimisation table for the reduction of picric acid

Sr. no.	Substrate (mg)	Catalyst loading	$NaBH_4$ (mg)	Time (min)
1	23 mg	30 mg	19	01:57
2	23 mg	30 mg	28	01:05
3	23 mg	30 mg	38	00:45
4	23 mg	20 mg	19	01:35
5	23 mg	20 mg	28	00:56
6	23 mg	20 mg	38	00:45
7	23 mg	10 mg	19	02:19
8	23 mg	10 mg	28	01:48
9	23 mg	10 mg	38	01:20
10	23 mg	No catalyst	19	No reaction

Table 4 Optimisation table for the reduction of 4-nitroaniline

Sr. no.	Substrate (mg)	Catalyst loading	$NaBH_4$ (mg)	Time (min)
1	14 mg	30 mg	19	01:05
2	14 mg	30 mg	28	00:40
3	14 mg	30 mg	38	00:25
4	14 mg	20 mg	19	01:54
5	14 mg	20 mg	28	01:31
6	14 mg	20 mg	38	01:15
7	14 mg	10 mg	19	03:25
8	14 mg	10 mg	28	01:45
9	14 mg	10 mg	38	01:34
10	14 mg	Without catalyst	19	No reaction

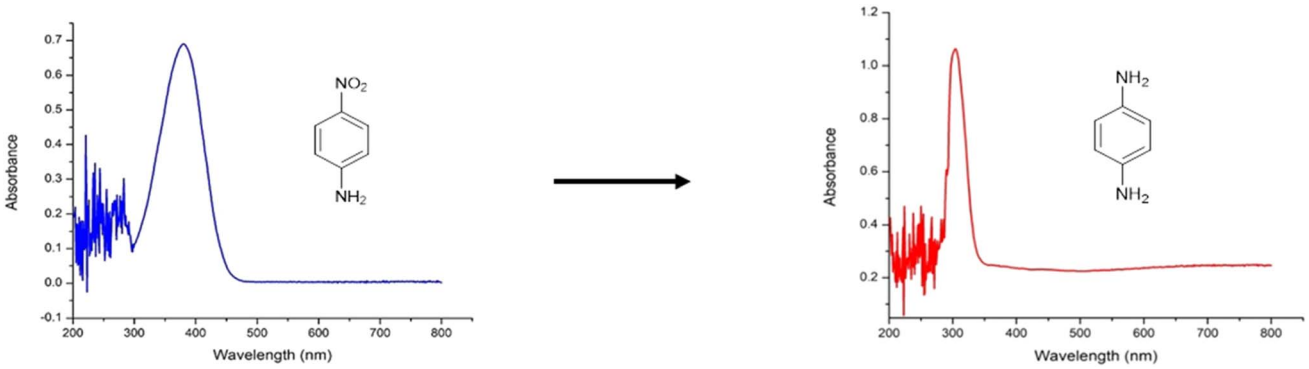

Fig. 8 Reduction of 4-nitroaniline.

the peak shifts to 297 nm due to the formation of *p*-amino phenol. Complete reduction of *p*-nitrophenol was takes place within 1:40 minutes with 30 mg of catalyst and 19 mg of sodium borohydride (Table 2, entry 1). While a high quantity of $NaBH_4$ requires less time, *i.e.*, 1:10 minutes for the complete reduction (Table 1, entry 3). As shown in Fig. 9(a), there is no reduction observed in the absence of catalyst (Table 2, entry 10).

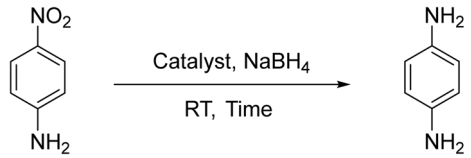

Scheme 6 Catalytic reduction of 4-nitroaniline.

4.2 Picric acid

Picric acid show absorbance at 354 nm in the absence of catalyst and $NaBH_4$. This peak shits to 300 due to formation of picramic acid (Fig. 7).[60] Such a reduction was observed in the presence of the catalyst and $NaBH_4$, and without catalyst, the reduction of picric acid was not observed (Table 3, entry 10). 19 mg of $NaBH_4$ with 30 mg of catalyst were required 1 minute

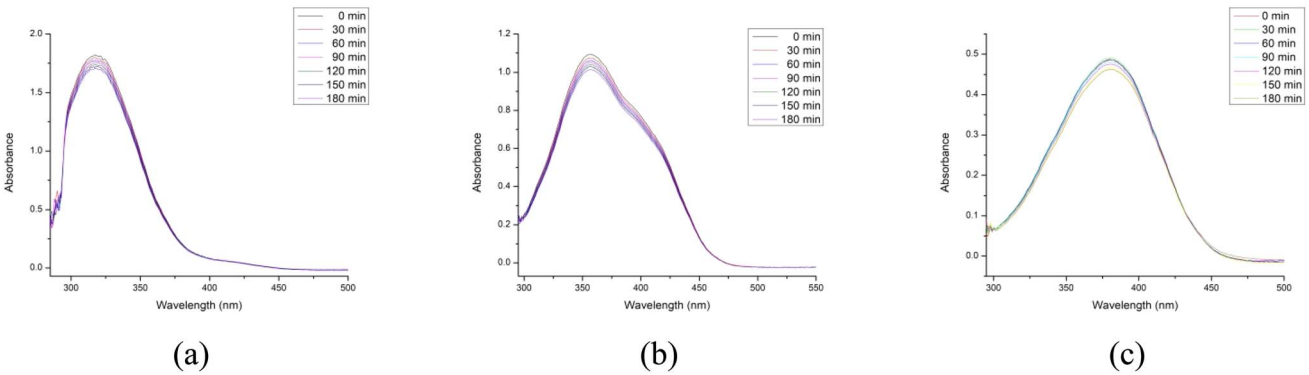

Fig. 9 Reduction of (a) 4-nitrophenol, (b) picric acid and (c) 4-nitroaniline in the absence of $NaBH_4$.

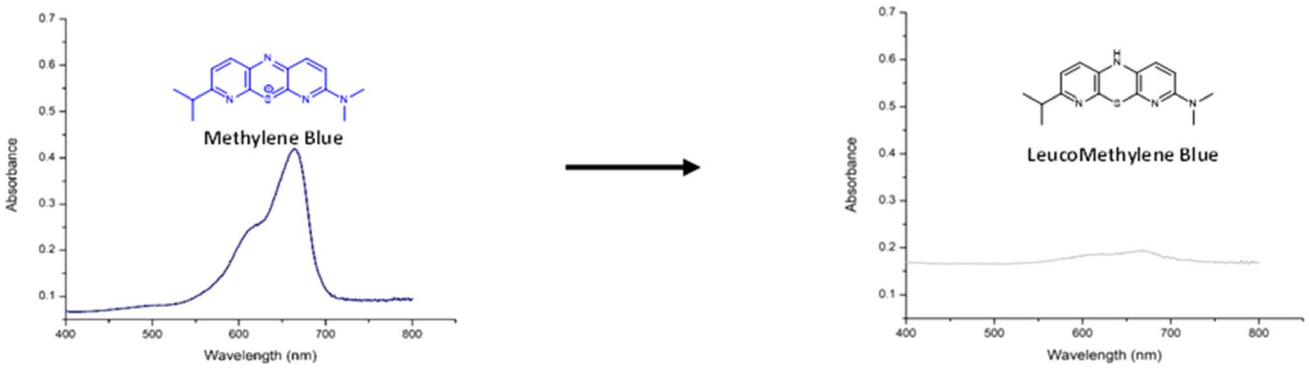

Fig. 10 Reduction of methylene blue.

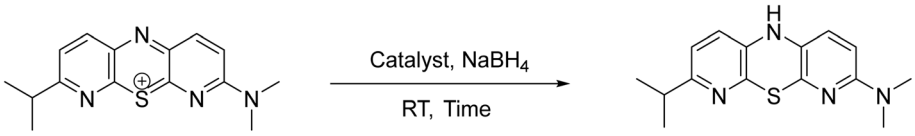

Scheme 7 Reduction of methylene blue.

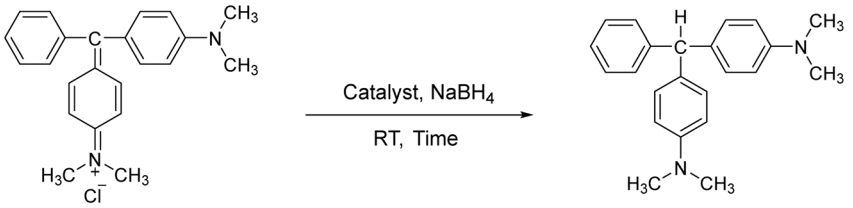

Scheme 8 Reduction of malachite green.

and 57 seconds for the reduction of picric acid (Table 3, entry 1) and only 45 seconds is required for the complete reduction of picric acid with 38 mg of $NaBH_4$ with 30 mg of catalyst (Table 3, entry 3). As well as the amount of catalyst decreases, the required time for the reduction of picric acid increases (Table 3, entries 4–9) and reduction not observed in the absence of catalyst (Fig. 9(b)).

4.3 4-Nitroaniline

As shown in Fig. 8, the UV-visible spectra demonstrate the reduction of 4-nitroaniline to 1,4 diamino benzene (Scheme 6). At initial time, 4-nitroaniline exhibited the absorbance at 380 nm and intensity of this peak decreased and shifts to 305 nm due to complete reduction which is observed after 1:05 minutes with 30 mg of catalyst and 19 mg of $NaBH_4$ (Table 4). Without catalyst, reduction of 4-nitroaniline is not reduced as shown in Fig. 9(c).

4.4 Methylene blue

Methylene blue is widely used in the textile industry. UV-visible spectra for methylene blue is observed at 665 nm.[42] As shown in Fig. 10, the intensity of the peak decreases after reaction with $NaBH_4$ and the catalyst. Such reduction occurs instantaneously as shown in Scheme 7.

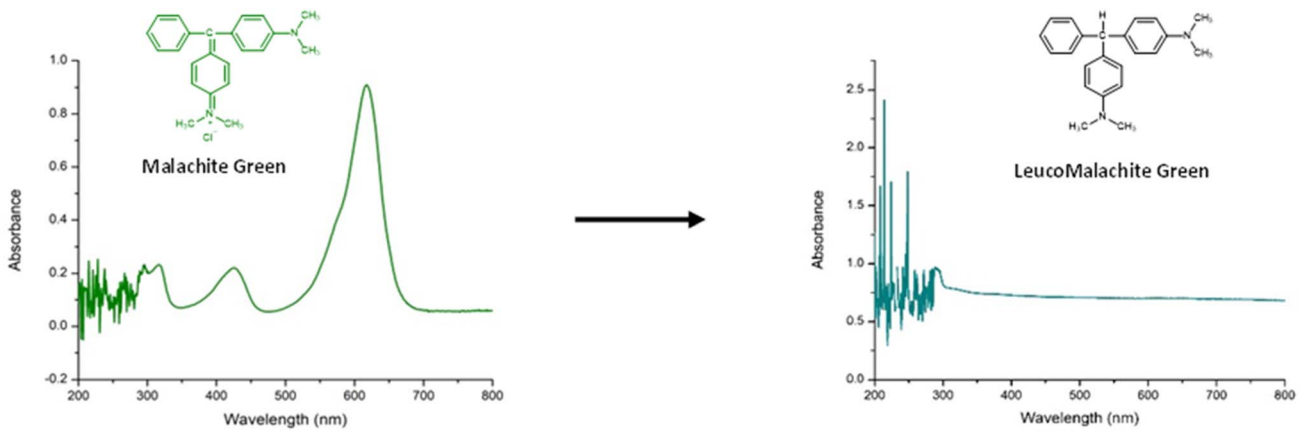

Fig. 11 Reduction of malachite green.

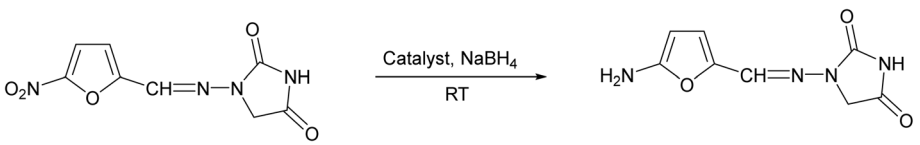

Scheme 9 Reduction of nitrofurantoin.

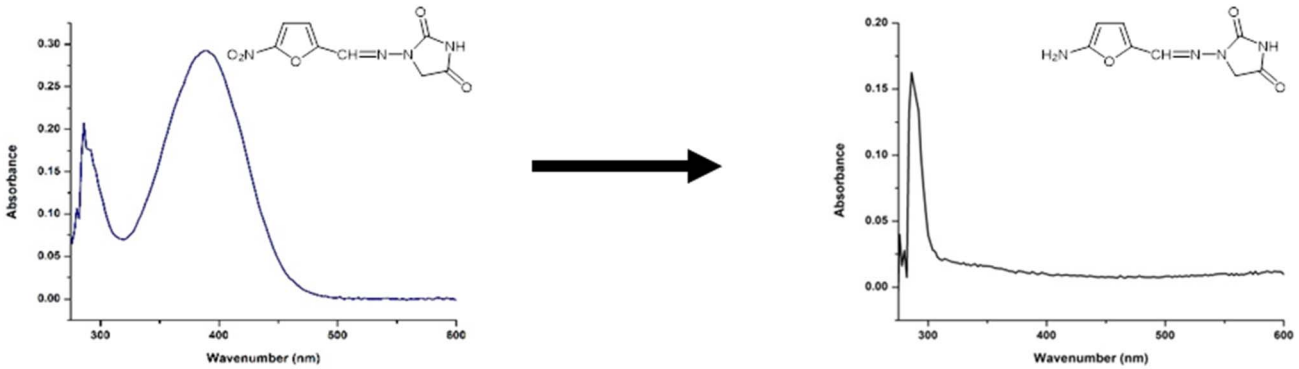

Fig. 12 Reduction of nitrofurantoin.

4.5 Malachite green

The UV-visible spectra for malachite green exhibit at 426 and 617 nm. As shown in Scheme 8, it gets disappeared after adding of 38 mg of $NaBH_4$ and 20 mg of catalyst instantly (Fig. 11).[65]

4.6 Nitrofurantoin

Nitrofurantoin also used for the reduction reaction to explore the potential of Ni-MOF/GO (10 mg) at room temperature using $NaBH_4$ (9 mg) as a reducing agent. Initially, the UV peak was observed at 380 nm for fresh nitrofurantoin. After 5 min, UV peak is getting disappeared which shows the complete reduction of nitrofurantoin (Scheme 9 and Fig. 12).

4.7 Mechanism for reduction of nitro compounds

A possible mechanism for the reduction of nitroaromatic compounds is shown in Scheme 10. It is multistep process which involves: (a) adsorption of hydrogen ions released form $NaBH_4$, (b) adsorption of nitroaromatics on the surface of synthesized catalyst, (c) transfer of electron by the surface of catalyst from BH_4^- to nitroaromatics and (d) desorption of reduced aromatic amino compounds.

The process begins with the nitro group being reduced to *N*-hydroxylamine oxide *via* hydride addition at the oxygen. $NaBH_4$, is employed as a nucleophile in order to facilitate electron transfer and BH_4^- binds to the surface of composite and electron transfer to surface of composite subsequently. Such type of

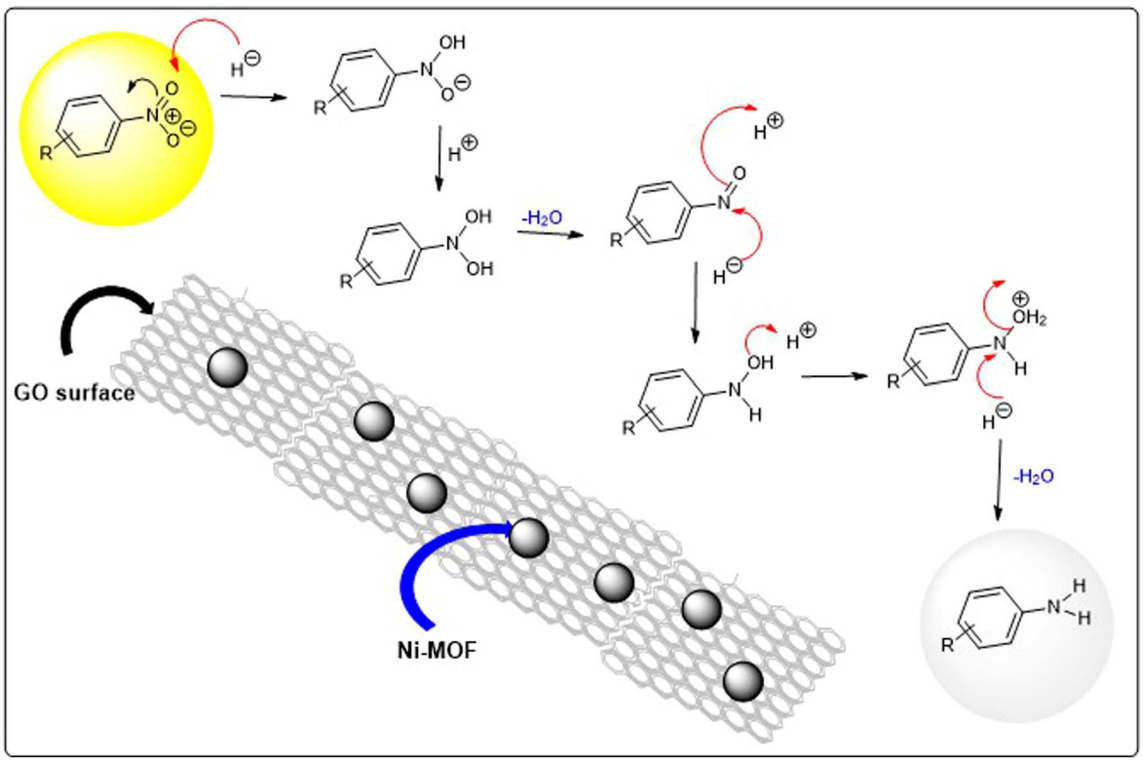

Scheme 10 Possible mechanism for the reduction of nitroaromatic compounds.

Table 5 Structure of nitro aromatic compounds and dyes with their possible product formed after the reduction[a]

Organic pollutant	Product	λ_{max} (nm) at initial time	λ_{max} (nm) of final product formed
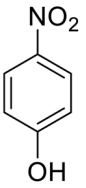	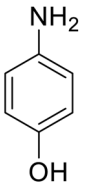	317	299
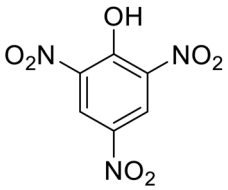	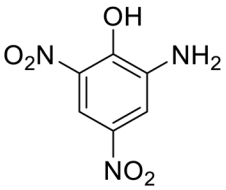	354	300
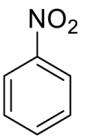	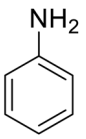	270	280
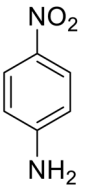	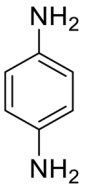	380	305
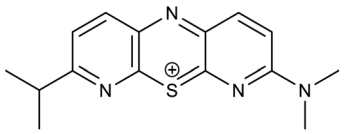	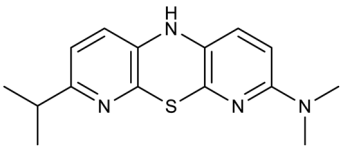	665	Disappeared
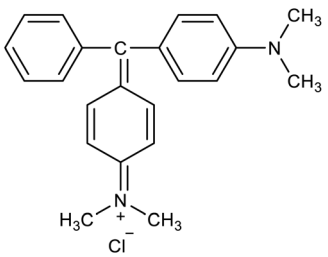	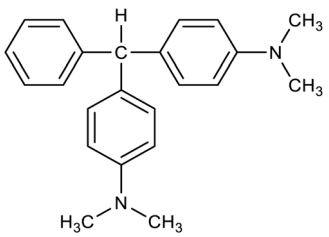	617, 426	Disappeared
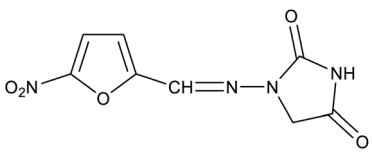	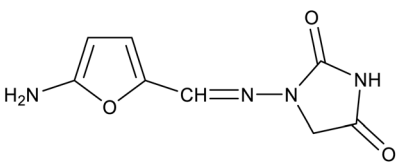	380	Disappeared

[a] UV spectra analysis of nitroaromatic compounds and dyes.

electron transfer accelerates the conversion of nitro group to amino group.[66] In next step, the *N*-hydroxylamine oxide is further reduced to dihydroxylamine, which then forms a nitroso group through the loss of water. The nitroso group is subsequently reduced to the amino product by hydrogen addition across the double bond. The final amino product is released from the surface of the Ni-MOF/GO composite into the solution, as confirmed by UV-visible spectroscopy. Thus, the primary steps in the reduction include reactant adsorption onto the catalyst, reduction of the nitro group to an amino group, and

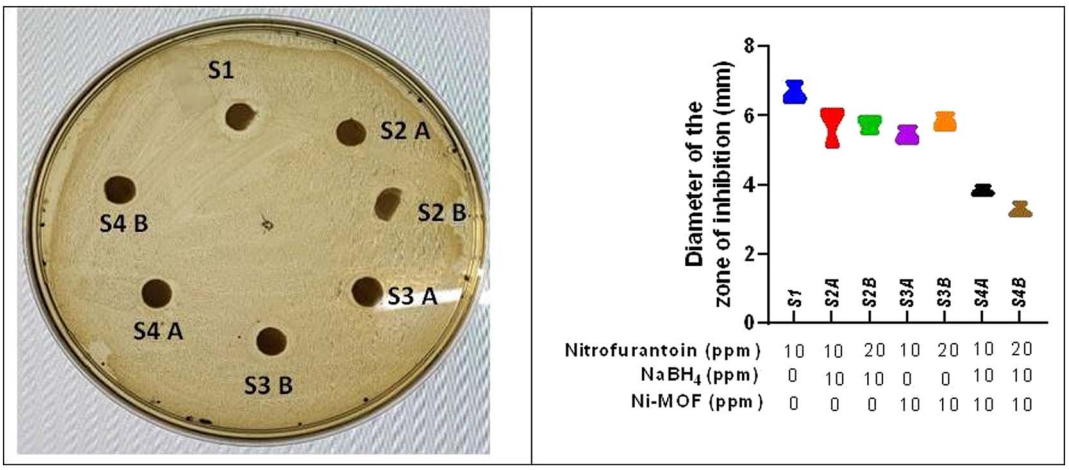

Fig. 13 Antibiotic activity assay for nitrofurantoin: (A) image of the agar plate indicating the zone of inhibition around the disk of filter paper over which the antibiotic solution was deposited. A larger zone of inhibition indicates activity of the antibiotic to inhibit the growth of *E. coli* bacteria which was spread over the plate just before the addition of the antibiotic. (B) A violin plot indicating the radius of the zone of inhibition in different samples.

desorption of the product from the catalyst surface. The reduction of nitroaromatic compounds and dyes was observed and the results are shown in Table 5, which compares the absorption peaks before and after reduction.

4.8 Biological activity of reduced nitrofurantoin

As shown in Fig. 13, nitrofurantoin shows the biological activity against *E. coli*. After reduction with catalyst and $NaBH_4$, the biological activity disappeared. We also observed the effect of only the catalyst and only $NaBH_4$, there is no significant biological activity observed against *E. coli*. Catalytic system of Ni-MOF/GO and $NaBH_4$ may be used as the reduction of nitrofurantoin to eliminate or stop the resistance of bacteria against the antibiotic drug.

5. Conclusion

The study successfully demonstrates the synthesis and application of the Ni-MOF/GO composite as a efficient catalyst for the reduction of nitroaromatic compounds such as *p*-nitrophenol (PNP), picric acid, *p*-nitroaniline (PNA), methylene blue, malachite green and nitrofurantoin. The catalyst exhibited excellent performance with all the pollutants and nitrofurantoin, primarily due to the large surface area and uniform distribution of Ni-MOF nanoparticles on the GO sheets. This distribution enhanced the interaction between the reactants and the catalyst, leading to faster and more efficient reduction reactions. Moreover, the Ni-MOF/GO composite was shown to be a promising alternative to traditional catalysts, offering improved reaction times, stability, and reusability, making it a potential candidate for industrial applications involving the reduction of nitroaromatic pollutants. Prepared catalyst is characterized by using SEM, HR-TEM, XRD, and FTIR. In addition, reduction reactions were confirmed by UV-vis spectroscopy.

Conflicts of interest

The authors declare that there no conflicts of interest.

Data availability

Data will be available from corresponding author on request.

Supplementary information (SI) is available. See DOI: https://doi.org/10.1039/d6ra00044d.

Acknowledgements

Authors acknowledged the FI2/(Project-282) RSPCB/Project/3491–3495 for the financial support.

References

1 C. Hu, L. Zhang and J. Gong, Recent progress made in the mechanism comprehension and design of electrocatalysts for alkaline water splitting, *Energy Environ. Sci.*, 2019, **12**(9), 2620–2645.

2 S. H. Mir, P. M. Hasan, E. Y. Danish and M. Aslam, Pd-induced phase separation in poly (methyl methacrylate) telopolymer: synthesis of nanostructured catalytic Pd nanorods, *Colloid Polym. Sci.*, 2020, **298**(4), 441–448.

3 T. Wu, H. Zheng, Y. Kou, X. Su, N. R. Kadasala, M. Gao, L. Chen, D. Han, Y. Liu and J. Yang, Self-sustainable and recyclable ternary Au@Cu_2O–Ag nanocomposites: application in ultrasensitive SERS detection and highly efficient photocatalysis of organic dyes under visible light, *Microsyst. Nanoeng.*, 2021, **7**(1), 23.

4 H. Xu, S. Wang, M. Wang, B. Ge, G. Ren, W. Li and L. Zhao, Application of superhydrophobic ZnO rod composites with environmentally-friendly and photodegradation properties in water environment treatment, *Colloids Surf., A*, 2021, **618**, 126437.

5 T. Liu, Y. Sun, B. Jiang, W. Guo, W. Qin, Y. Xie, B. Zhao, L. Zhao, Z. Liang and L. Jiang, Pd nanoparticle-decorated 3D-printed hierarchically porous TiO_2 scaffolds for the efficient reduction of a highly concentrated 4-nitrophenol solution, *ACS Appl. Mater. Interfaces*, 2020, **12**(25), 28100–28109.

6 X. Kang, D. Teng, S. Wu, Z. Tian, J. Liu, P. Li, Y. Ma and C. Liang, Ultrafine copper nanoparticles anchored on reduced graphene oxide present excellent catalytic performance toward 4-nitrophenol reduction, *J. Colloid Interface Sci.*, 2020, **566**, 265–270.

7 X. Zhao, X. Liu, C. Yi, J. Li, Y. Su and M. Guo, Palladium nanoparticles embedded in yolk–shell N-doped carbon nanosphere@ void@SnO_2 composite nanoparticles for the photocatalytic reduction of 4-nitrophenol, *ACS Appl. Nano Mater.*, 2020, **3**(7), 6574–6583.

8 X. Zhao, X. Liu, C. Yi, J. Li, Y. Su and M. Guo, Palladium nanoparticles embedded in yolk–shell N-doped carbon nanosphere@ void@SnO_2 composite nanoparticles for the photocatalytic reduction of 4-nitrophenol, *ACS Appl. Nano Mater.*, 2020, **3**(7), 6574–6583.

9 K. Layek, M. L. Kantam, M. Shirai, D. Nishio-Hamane, T. Sasaki and H. Maheswaran, Gold nanoparticles stabilized on nanocrystalline magnesium oxide as an active catalyst for reduction of nitroarenes in aqueous medium at room temperature, *Green Chem.*, 2012, **14**(11), 3164–3174.

10 H. Zhang and X. Hu, Preparation of Fe_3O_4-rGO via a covalent chemical combination method and its catalytic performance on p-NP bioreduction, *J. Environ. Chem. Eng.*, 2017, **5**(4), 3348–3353.

11 K. J. Datta, A. K. Rathi, P. Kumar, J. Kaslik, I. Medrik, V. Ranc, R. S. Varma, R. Zboril and M. B. Gawande, Synthesis of flower-like magnetite nanoassembly: application in the efficient reduction of nitroarenes, *Sci. Rep.*, 2017, **7**(1), 11585.

12 B. H. Hameed, A. L. Ahmad and K. N. Latiff, Adsorption of basic dye (methylene blue) onto activated carbon prepared from rattan sawdust, *Dyes Pigments*, 2007, **75**(1), 143–149.

13 R. Kulkarni, S. Harip, A. R. Kumar, D. Deobagkar and S. Zinjarde, Peptide stabilized gold and silver nanoparticles derived from the mangrove isolate Pseudoalteromonas lipolytica mediate dye decolorization, *Colloids Surf., A*, 2018, **555**, 180–190.

14 W. C. Wanyonyi, J. M. Onyari and P. M. Shiundu, Adsorption of Congo red dye from aqueous solutions using roots of Eichhornia crassipes: kinetic and equilibrium studies, *Energy Procedia*, 2014, **50**, 862–869.

15 H. Huo, Y. Jiang, Z. Wang, Y. Hu, T. Zhao, X. Liu, X. Xu and K. Lin, Carbonyl oxygen-coordinated metallic cobalt nanoparticles anchored on hybrid mesoporous silica matrix to enhance 4-nitrophenol hydrogenation, *J. Mater. Sci.*, 2021, **56**(1), 364–379.

16 R. D. Neal, R. A. Hughes, P. Sapkota, S. Ptasinska and S. Neretina, Effect of nanoparticle ligands on 4-nitrophenol reduction: Reaction rate, induction time, and ligand desorption, *ACS Catal.*, 2020, **10**(17), 10040–10050.

17 H. Zheng, J. Huang, T. Zhou, Y. Jiang, Y. Jiang, M. Gao and Y. Liu, Recyclable magnetic Cu/CuFe2O4 nanocomposites for the rapid degradation of 4-NP, *Catalysts*, 2020, **10**(12), 1437.

18 J. Strachan, C. Barnett, A. F. Masters and T. Maschmeyer, 4-Nitrophenol reduction: probing the putative mechanism of the model reaction, *ACS Catal.*, 2020, **10**(10), 5516–5521.

19 J. Tokuda, R. Ohura, T. Iwasaki, Y. Takeuchi, A. Kashiwada and M. Nango, Decoloration of azo dyes by hydrogen peroxide catalyzed by water-soluble manganese porphyrins, *Text. Res. J.*, 1999, **69**(12), 956–960.

20 G. Gordon, R. D. Gauw, Y. Miyahara, B. Walters and B. Bubnis, Using indigo absorbance to calculate the indigo sensitivity coefficient, *J. - Am. Water Works Assoc.*, 2000, **92**(12), 96–100.

21 H. Bader and J. Hoigné, Determination of ozone in water by the indigo method, *Water Res.*, 1981, **15**(4), 449–456.

22 J. Poulin, Identification of indigo and its degradation products on a silk textile fragment using gas chromatography-mass spectrometry, *J. CAC*, 2007, **32**, 48–56.

23 C. Iuga, E. Ortiz, J. R. Alvarez-Idaboy and A. Vivier-Bunge, Molecular description of indigo oxidation mechanisms initiated by OH and OOH radicals, *J. Phys. Chem.*, 2012, **116**(14), 3643–3651.

24 D. Brown, Effects of colorants in the aquatic environment, *Ecotoxicol. Environ. Saf.*, 1987, **13**(2), 139–147.

25 F. Ding, W. Liu, J. X. Diao and Y. Sun, Characterization of Alizarin Red S binding sites and structural changes on human serum albumin: a biophysical study, *J. Hazard Mater.*, 2011, **186**(1), 352–359.

26 M. Ghaedi, A. Hassanzadeh and S. N. Kokhdan, Multiwalled carbon nanotubes as adsorbents for the kinetic and equilibrium study of the removal of alizarin red S and morin, *J. Chem. Eng. Data*, 2011, **56**(5), 2511–2520.

27 L. Gong, W. Sun and L. Kong, Adsorption of methylene blue by NaOH-modified dead leaves of plane trees. Computational Water, Energy, and, *Environ. Eng.*, 2013, **2**(2), 13–19.

28 P. Ngamsurach, S. Nemkhuntod, P. Chanaphan and P. Praipipat, Modified beaded materials from recycled wastes of bagasse and bagasse fly ash with iron (III) oxide-hydroxide and zinc oxide for the removal of reactive blue 4 dye in aqueous solution, *ACS Omega*, 2022, **7**(39), 34839–34857.

29 U. Gulati, U. C. Rajesh and D. S. Rawat, CuO/Fe_2O_3 NPs: robust and magnetically recoverable nanocatalyst for decarboxylative A3 and KA2 coupling reactions under neat conditions, *Tetrahedron Lett.*, 2016, **57**(40), 4468–4472.

30 S. Vigneswari, T. S. Amelia, M. H. Hazwan, G. K. Mouriya, K. Bhubalan, A. A. Amirul and S. Ramakrishna, Transformation of biowaste for medical applications: Incorporation of biologically derived silver nanoparticles as antimicrobial coating, *Antibiotics*, 2021, **10**(3), 229.

31 J. Xu, Y. Bi, H. Zhao, L. Shi, N. Zhang and X. Xin, In situ synthesis of well-dispersed silver nanoparticles from silver nanoclusters hydrogel for catalytic reduction of 4-Nitrophenol, *Appl. Surf. Sci.*, 2025, **683**, 161759.

32 D. Mangindaan, G. Y. Lin, C. J. Kuo and H. W. Chien, Biosynthesis of silver nanoparticles as catalyst by spent coffee ground/recycled poly (ethylene terephthalate) composites, *Food Bioprod. Process.*, 2020, **121**, 193–201.

33 T. Deng, J. Wu and H. Cheng, Biosynthesis of silver nanocatalyst as a highly active catalyst towards reduction of 4-nitrophenol and dyes contaminate and investigation of its anti-uveal melanoma properties, *Inorg. Chem. Commun.*, 2024, **162**, 112001.

34 M. Ezazi, K. Asadpour-Zeynali and E. Saeb, Synergistic incorporation of Ag into nickel hydroxide nanostructure to enhance the electroctrocatalytic determination of nitrofurantoin, *Inorg. Chem. Commun.*, 2024, **160**, 111913.

35 J. Wen, Decorated of silver nanoparticles over Lignin-Chitosan composite: evaluating its effectiveness in reducing nitro compounds and amelioration the Antibiotic-Associated diarrhea induced by Lincomycin hydrochloride in rats via following the MAPK signaling pathways, *J. Polym. Environ.*, 2025, **33**(4), 1916–1933.

36 M. Ghosh, J. Liu, S. S. Chuang and S. C. Jana, Fabrication of hierarchical V_2O_5 nanorods on TiO_2 nanofibers and their enhanced photocatalytic activity under visible light, *ChemCatChem*, 2018, **10**(15), 3305–3318.

37 K. Zeng, X. Li, C. Wang, Z. Wang, P. Guo, J. Yu, C. Zhang and X. S. Zhao, Three-dimensionally macroporous MnZrOx catalysts for propane combustion: Synergistic structure and doping effects on physicochemical and catalytic properties, *J. Colloid Interface Sci.*, 2020, **572**, 281–296.

38 K. Zeng, Z. Wang, D. Wang, C. Wang, J. Yu, G. Wu, Q. Zhang, X. Li, C. Zhang and X. S. Zhao, Three-dimensionally ordered macroporous MnSmOx composite oxides for propane combustion: Modification effect of Sm dopant, *Catal. Today*, 2021, **376**, 211–221.

39 K. Zeng, Z. Wang, D. Wang, C. Wang, J. Yu, G. Wu, Q. Zhang, X. Li, C. Zhang and X. S. Zhao, Three-dimensionally ordered macroporous MnSmOx composite oxides for propane combustion: Modification effect of Sm dopant, *Catal. Today*, 2021, **376**, 211–221.

40 X. Ma, X. Yu and M. Ge, Highly efficient catalytic oxidation of benzene over Ag assisted Co_3O_4 catalysts, *Catal. Today*, 2021, **376**, 262–268.

41 S. Dissanayake, N. Wasalathanthri, A. S. Amin, J. He, S. Poges, D. Rathnayake and S. L. Suib, Mesoporous Co_3O_4 catalysts for VOC elimination: Oxidation of 2-propanol, *Appl. Catal., A*, 2020, **590**, 117366.

42 V. S. Suvith, V. S. Devu and D. Philip, Facile synthesis of SnO_2/NiO nano-composites: Structural, magnetic and catalytic properties, *Ceram. Int.*, 2020, **46**(1), 786–794.

43 K. Sharma, P. Raizada, A. Hosseini-Bandegharaei, P. Thakur, R. Kumar, V. K. Thakur, V. H. Nguyen and S. Pardeep, Fabrication of efficient CuO/graphitic carbon nitride based heterogeneous photo-Fenton like catalyst for degradation of 2, 4 dimethyl phenol, *Process Saf. Environ. Prot.*, 2020, **142**, 63–75.

44 C. Cai, Z. Zhang, J. Liu, N. Shan, H. Zhang and D. D. Dionysiou, Visible light-assisted heterogeneous Fenton with $ZnFe_2O_4$ for the degradation of Orange II in water, *Appl. Catal., B*, 2016, **182**, 456–468.

45 A. Gulati, J. Malik and R. Kakkar, Mesoporous rGO@ZnO composite: Facile synthesis and excellent water treatment performance by pesticide adsorption and catalytic oxidative dye degradation, *Chem. Eng. Res. Des.*, 2020, **160**, 254–263.

46 X. Huang, X. Zhou, S. Wu, Y. Wei, X. Qi, J. Zhang, F. Boey and H. Zhang, Reduced graphene oxide-templated photochemical synthesis and in situ assembly of Au nanodots to orderly patterned Au nanodot chains, *Small*, 2010, **6**(4), 513–516.

47 J. Huang, L. Zhang, B. Chen, N. Ji, F. Chen, Y. Zhang and Z. Zhang, Nanocomposites of size-controlled gold nanoparticles and graphene oxide: formation and applications in SERS and catalysis, *Nanoscale*, 2010, **2**(12), 2733–2738.

48 H. Wei and E. Wang, Nanomaterials with enzyme-like characteristics (nanozymes): next-generation artificial enzymes, *Chem. Soc. Rev.*, 2013, **42**(14), 6060–6093.

49 N. Bagheri, M. Dastborhan, A. Khataee, J. Hassanzadeh and M. Kobya, Synthesis of g-C_3N_4@ CuMOFs nanocomposite with superior peroxidase mimetic activity for the fluorometric measurement of glucose, *Spectrochim. Acta, Part A*, 2019, **213**, 28–36.

50 R. Wang, H. Xu, K. Zhang, S. Wei and W. Deyong, High-quality Al@ Fe-MOF prepared using Fe-MOF as a micro-reactor to improve adsorption performance for selenite, *J. Hazard Mater.*, 2019, **364**, 272–280.

51 Y. Liu, G. Jia, Q. Wu, D. Zhang, J. Wu, Y. Yin, S. Sai, Z. Guo and X. Cui, MOF-derived FeNiCoOX hierarchical hollow nanocages for oxygen evolution reaction, *Mater. Lett.*, 2021, **291**, 129564.

52 C. Zhang, S. Wei, L. Sun, F. Xu, P. Huang and H. Peng, Synthesis, structure and photocatalysis properties of two 3D Isostructural Ln (III)-MOFs based 2, 6-Pyridinedicarboxylic acid, *J. Mater. Sci. Technol.*, 2018, **34**(9), 1526–1531.

53 Y. Chen, D. Lv, J. Wu, J. Xiao, H. Xi, Q. Xia and Z. Li, A new MOF-505@ GO composite with high selectivity for CO_2/CH_4 and CO_2/N_2 separation, *Chem. Eng. J.*, 2017, **308**, 1065–1072.

54 Z. Hasan, D. W. Cho, G. J. Islam and H. Song, Catalytic decoloration of commercial azo dyes by copper-carbon composites derived from metal organic frameworks, *J. Alloys Compd.*, 2016, **689**, 625–631.

55 Y. Chen, B. Zhai, Y. Liang, Y. Li and J. Li, Preparation of CdS/g-C_3N_4/MOF composite with enhanced visible-light photocatalytic activity for dye degradation, *J. Solid State Chem.*, 2019, **274**, 32–39.

56 G. Pandey, N. Singh, N. Rajput, M. K. Saini, S. L. Kothari, J. Prasad, N. P. Lamba and M. S. Chauhan, Comparative study of NiO/CuO/Ag doped graphene based materials for reduction of nitroaromatic compounds and degradation of dye with statistical study, *Sci. Rep.*, 2024, **14**(1), 2077.

57 J. Gao, P. He, T. Yang, X. Wang, L. Zhou, Q. He, L. Jia, H. Deng, H Zhang, B. Jia and X. He, Short rod-like Ni-MOF anchored on graphene oxide nanosheets: A

promisingvoltammetric platform for highly sensitive determination of pchloronitrobenzene, *J. Electroanal. Chem.*, 2020, **861**, 113954.

58 S. Gao, Y. Sui, F. Wei, J. Qi, Q. Meng and Y. He, Facile synthesis of nickel metal–organic framework derived hexagonal flaky NiO for supercapacitors, *J. Mater. Sci.: Mater. Electron.*, 2018, **29**(3), 2477–2483.

59 M. S. More, G. A. Bodkhe, N. N. Ingle, F. Singh, M. L. Tsai, M. Kim and M. D. Shirsat, Metal-organic framework (MOF)/reduced graphene oxide (rGO) composite for high performance CO sensor, *Solid-State Electron.*, 2023, **204**, 108638.

60 R. Verma, M. S. Chauhan, S. Pandey and A. Dandia, Reduced graphene Oxide/NiO based nano-composites for the efficient removal of alizarin dye, indigo dye and reduction of nitro aromatic compounds, *Heliyon*, 2023, **9**(6), e17162.

61 B. Baruah, G. J. Gabriel, M. J. Akbashev and M. E. Booher, Facile synthesis of silver nanoparticles stabilized by cationic polynorbornenes and their catalytic activity in 4-nitrophenol reduction, *Langmuir*, 2013, **29**(13), 4225–4234.

62 Y. Liu, H. Xu, H. Yu, H. Yang and T. Chen, Synthesis of lignin-derived nitrogen-doped carbon as a novel catalyst for 4-NP reduction evaluation, *Sci. Rep.*, 2020, **10**(1), 20075.

63 J. Xia, G. He, L. Zhang, X. Sun and X. Wang, Hydrogenation of nitrophenols catalyzed by carbon black-supported nickel nanoparticles under mild conditions, *Appl. Catal., B*, 2016, **180**, 408–415.

64 M. A. Bhosale, D. R. Chenna and B. M. Bhanage, Ultrasound assisted synthesis of gold nanoparticles as an efficient catalyst for reduction of various nitro compounds, *ChemistrySelect*, 2017, **2**(3), 1225–1231.

65 S. Mastoi, M. A. Bhatti, A. Tahira, M. A. Jakhrani, A. Manan, S. Kumar, A. A. Shah, A. Nafady, A. Liaquat, E. A. Dawi and A. A. Ismail, Efficient photodegradation of malachite green in sunlight using ZnO nanostructures modified with pomegranate peel, *J. Mater. Sci.: Mater. Electron.*, 2023, **34**(28), 1943.

66 R. Wang, C. Cai, D. Wang, Z. Liu, L. Gao and T. Jiao, Self-assembled Au/Fe_3O_4 nanoparticle-loaded phytic acid-graphene oxide composite foam with highly efficient catalytic performance for p-nitrophenol and o-nitroaniline organic pollutants, *Colloids Surf., A*, 2021, **617**, 126368.